Disorder-to-order transition in selenium under cyclic compression-decompression

Xingbang Dong,[1,*] Kaiyuan Shi,[1,*] Jiaqing Zhang,[1,*] Wenbo Fu,[1,*] Zhaoxu Du,[1] Haotian Yang,[1] Jun Kong,[1] Pu Qiao,[1] Xin Zhang,[1] and Lei Su[1,2,†]

[1]*Center for High Pressure Science and Technology Advanced Research, Beijing 100093, China*

[2]*Shanghai Advanced Research in Physical Sciences, Shanghai 201203, China*

(Received 17 October 2024; revised 26 January 2025; accepted 30 January 2025; published 10 February 2025)

Amorphous solids, as long-range disorder materials, have complex order on multiple length scales. The regulation of the degree of order is generally achieved through annealing or static compression. Unlike previous studies, this work has triggered the disorder-to-order transition in amorphous selenium (*a*-Se) by cyclic compression-decompression in a dynamic diamond anvil cell. We found that the degree of order in the directionally bonded *a*-Se positively correlates with the number of compression cycles, and long-range order was achieved in a relatively low-pressure range. The possible transformation mechanism is discussed on the basis of medium-range structural parameter regulation. This work provides an understanding of the relaxation and extension of the order length scale by unconventional mechanical stimulation.

DOI: 10.1103/PhysRevB.111.064105

I. INTRODUCTION

Amorphous solids refer to materials that do not possess long-range order. Unlike their crystalline counterpart, they have complex orders on multiple length scales, and the degree of order can be readily modified between different structural orders by annealing and static compression [1–6]. Furthermore, amorphous solids are very sensitive to fabrication history. Several research groups have reported different experimental and theoretical results under the same composition, implying that the local atomic rearrangement and degree of disorder could be different and fluctuate to some extent [7–10]. After decades of research effort, identifying and regulating the of degree of order on the length scales in amorphous solids has been extended to a medium-range order (MRO) and even to a long-range topological order [11,12]. Nevertheless, general insight into the extended length scale from the short-range order (SRO) to long-range order (LRO) remains much more limited, including the formation and/or connectivity of the extended structure order.

While static compression can regulate the degree of order in amorphous solids, it may delay or hinder the structural order on the extended length as the density increases and the static structural disorder fluctuates [13]. The recently developed dynamic diamond anvil cells (dDAC) may reduce this limitation and provide programmable compression-decompression cycles, including the programmed number of loading cycles and pressure amplitude [14]. Indeed, such dynamic compression-decompression methods can significantly manipulate the structure of many material systems, not only by accurately tuning the stress state of the compressed materials but also by realizing their multiple loading history under a wide magnitude of ramp rates within several to thousand GPa/s [15,16]. Therefore, this strategy allows the degree of order in amorphous solids to be modulated via nonequilibrium reciprocating compression. Previous reports show that some colloids and jammed systems exhibit structural ordering under oscillating shear strain. However, the interaction between particles is often ignored [17–20], which is really important in directionally bonded disordered systems. Generally, the structural rearrangement of covalent glasses under stress is mediated through the rotation of atomic bonds or chains without changing the bond length [21]. Thus, this effect is expected to be enhanced by the regulation of the dDAC.

Amorphous selenium has been utilized to investigate the disorder-to-order transition, as it shows intriguing structural order behavior reported by different groups, indicating different degrees of order on limited length scales [10,22–27]. The atomic homogeneity and typical polymorphous crystallization highlight the key role the degree of order plays in the disorder-to-order transition. *a*-Se is mainly composed of a one-dimensional single-atom polymerization chain and is structurally constrained by bond-stretching forces between nearest neighbors and bond-bending forces between next-nearest neighbors [28]. The two constraints and the uncorrelated Se chains lead to a flexible network. Thus, different structural configurations of *a*-Se in space may be accessible from an energy landscape perspective, which has a great impact on the subsequent transformation of the structural order. Liu *et al.* reported that *a*-Se exhibited two-step dynamic crystallization under static compression of about 10 GPa and attributed this to the local configuration fluctuation under stress [10]. Therefore, could a new strategy use dynamic compression-decompression to control and regulate the structural order of the flexible network in *a*-Se as well?

In this work, we study the cyclic-compression behavior of *a*-Se, focusing on the effect of the number of periodic pressure oscillations. We found that the disorder-to-order transition in the directionally bonded *a*-Se positively correlated with the number of compression cycles. We discuss the possible mechanism of cyclic compression-induced LRO in *a*-Se based on

*These authors contributed equally to this work.
†Contact author: lei.su@sharps.ac.cn

regulating the medium-range structural parameter. This work demonstrates that the structural order of amorphous solid can be effectively modulated by the dDAC, which contributes to synthesizing the metastable state and explores the connectivity of the MRO in the disorder-order transition.

II. METHOD

Amorphous selenium with high purity was obtained by the melt quenching method. The amorphous nature of *a*-Se was examined by x-ray diffraction (XRD, Bruker D8 Venture), Raman spectroscopy, and TEM. The two-dimensional (2D) diffraction images were collected with a Photon II detector and a fixed-chi goniometer using an Ag $K\alpha$ radiation source with a wavelength of 0.560 86 Å. The exposure time for each frame was 500 s. High-purity CeO_2 powder was used to calibrate the geometrical parameters of the detector. The 2D diffraction images were transformed into the intensity pattern versus 2θ using DIOPTAS [29]. Raman spectra were measured using the Renishaw micro-Raman spectroscopy system (inVia Reflex, Renishaw) with a 785 nm laser. To avoid thermal-induced crystallization an extremely low excitation power and a shorter exposure time is required. Raman spectra were collected in backscattering geometry using a 1200 g/mm grating. Before the measurement, the system was calibrated by the Raman signal of silicon. The TEM characterization was operated at 200 KV (JEOL, JEM-2100) and a small angle was required to avoid photoinduced crystallization.

A. High-pressure experiment

The high-pressure (HP) experiments were performed using a diamond anvil cell (DAC) with a diamond culet of 300 μm or 400 μm. The *a*-Se sample and ruby were loaded into a hole with a diameter of 180 μm and a thickness of 50 μm (preindented) in a steel gasket. The pressure was determined via the shift of the ruby R_1 emission line and the pressure difference is less than 2% [30]. The pressure was modulated by controlling prepressed screw during the compression-decompression cycles. No pressure-transmitting medium was used. The Raman mapping spectrum and XRD patterns of samples were collected after each period of cyclic loading. The samples were sealed in the DAC, with pressure released to ambient conditions, allowing for a clear comparison of the structural changes in *a*-Se before and after each loading cycle. Both acquisition parameters were set consistently with the above atmospheric pressure measurements.

B. Dynamic diamond anvil cell system

The dynamic diamond anvil cell system was combined with *in situ* fluorescence spectroscopy. Thus, the real-time pressure can be detected. The dynamic pressure was generated by the piezoelectric actuators (Nanomotions, Model PAL40VS25) combined with the above DAC. According to the output wave-form parameters of the function generator, the piezoelectric actuators dynamically adjusted the output voltage to control the pressure amplitude and loading rate. In this study, recording the output voltage was required to allow precise control of the pressure range. The periodic triangular wave form was used as the pressure tuning function, and

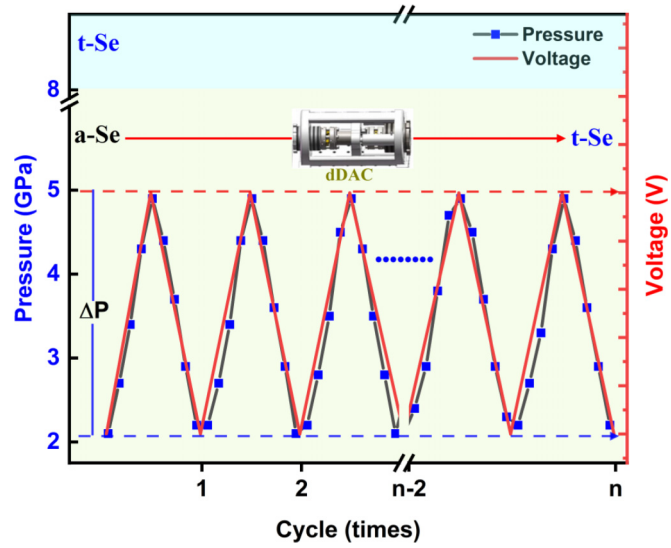

FIG. 1. Schematic diagram presents pressure oscillation as a function of the number of loading cycles. The number of cycles (n) is cumulative number of loading cycles (n) under specific pressure range (ΔP). The oscillation frequency is 5 Hz and the driving voltage obeys triangular wave form. The maximum pressure must be less than 8 GPa to avoid pressure-induced crystallization.

the loading frequency was 5 Hz. In order to maintain the stability of pressure amplitude, the homemade decompression attachments and double nut interlock were adopted, as shown in Fig. S1 in the Supplemental Material [33]. Several pressure cycles were performed in advance till the permanent plastic deformation of gasket and a double nut interlock were adopted to prevent the loosening of the prepressed screw. The good repeatability of pressure amplitude can be accessed and maximum pressure difference was less than 0.2 GPa during the whole cyclic compression-decompression, as shown in Fig. S1 in the Supplemental Material [33]. More detailed information about the dDAC system can be found in these reports [14,31,32].

III. RESULTS AND DISCUSSION

We demonstrate the validity of our hypothesis by showing our experimental results of the *a*-Se sample experiencing a disorder-to-order transition when subjected to a cumulative number of loading cycles (n) under specific pressure range (ΔP). The dynamic modulation of the pressure range as a function of n for the *a*-Se sample is shown in Fig. 1, where the certain pressure values are extracted from the experimental data shown in Fig. S1(a) in the Supplemental Material [33]. The periodic loading cycle and pressure change are modulated by repeating triangular wave forms. Prior to the study, the amorphous nature of *a*-Se was studied and confirmed by XRD analyses, Raman mapping spectrum, and High resolution TEM imaging, as shown in Fig. S2 in the Supplemental Material [33]. Note that the pressure value for each loading cycle is kept below 8 GPa to avoid crystallization, as confirmed in Fig. S3 in the Supplemental Material [33].

As shown in Fig. 2, the *a*-Se exhibits a disorder-to-order transition upon recovery after 3000 cycles within the cyclic

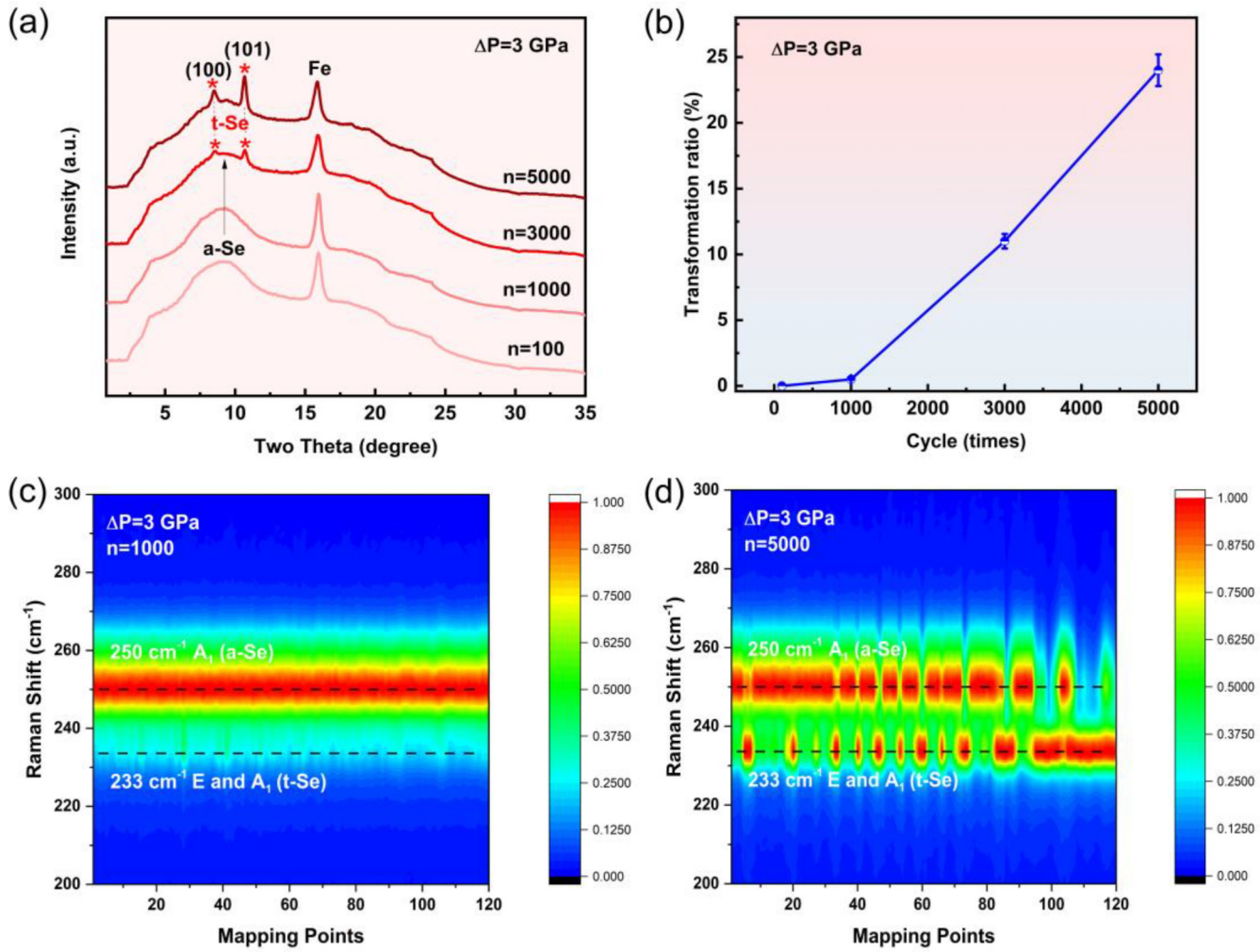

FIG. 2. Structure characterization of the recovered sample after different loading cycles under cyclic compression. (a) XRD characterization of the recovered sample at $\Delta P = 3$ GPa (2–5 GPa). (b) The relationship between the transformation ratio and the number of loading cycles at $\Delta P = 3$ GPa. The fitting error is less than 5%. (c), (d) Raman mapping characterization of recovered sample after $n = 1000$ and $n = 5000$ at $\Delta P = 3$ GPa (2–5 GPa), respectively.

pressure range 2–5 GPa ($n = 3000$, $\Delta P = 3$ GPa), as confirmed by the diffraction peaks (101) or (100) at about 8.5° or 10.7°. These new diffraction peaks can be well indexed to that of the trigonal selenium (t-Se) obtained by static compression diamond anvil cell (s-DAC) [10]. No obvious bright spot or texture can be detected in the raw 2D pattern, as shown in Fig. S4 in the Supplemental Material [33]. Furthermore, Raman mapping was performed, and the schematic image of the mapping region is shown in Fig. S5(c) in the Supplemental Material [33]. By comparing Figs. 2(c) and 2(d) with Fig. S5(d) in the Supplemental Material [33], a new Raman vibrational band (A_1 and E modes of t-Se) at around 233 cm^{-1} can be distinguished when the a-Se was recovered from $n = 3000$ or 5000. However, when the number of cycles was 100 and 1000 at $\Delta P = 3$ GPa, no obvious diffraction peaks can be detected, as confirmed in in Fig. 2(a), and further the peak shape/position of uncorrelated (Se)n chains (A_1 mode) at around 250 cm^{-1} remains unchanged, as shown in Fig. 2(c). In addition, it is worth noting that when ΔP is 2 or 1 GPa, no obvious crystallization signal can be observed from the XRD patterns even if the number of loading cycles reaches 5000, as shown in Figs. S5(a) and S5(b) in the Supplemental Material [33]. Furthermore, a-Se did not crystallize even when the number of cycles was increased up to 10 000 at $\Delta P = 2$ GPa and $\Delta P = 1$ GPa, although a small shoulder halo can be detected at about 10.7 ° for $\Delta P = 2$ GPa, as shown in Fig. S6 in the Supplemental Material [33]. The raw 2D pattern have been checked for $\Delta P = 2$ GPa that the scattered halo remains homogeneous. Compared with the above static compression (8 GPa), the threshold for the disorder-to-order transition of a-Se via dDAC is lower. The premature transformation demonstrates the strong effect of dynamic perturbation on the structure order and transformation kinetics of directionally bonded disordered solid.

Besides, the degree of the disorder-to-order transition of a-Se is positively correlated with n. As shown in Figs. 2(a), 2(c), and 2(d), the relative intensity of the diffraction peaks of t-Se and that of two Raman scattering bands (A_1 mode of a-Se at 250 cm^{-1} and A_1 and/or E mode of t-Se at 233 cm^{-1}) enhance with the increase in n from 3000 to 5000 at $\Delta P = 3$ GPa. Quantitative analysis was performed, as shown in Figs. S7 and S8 in the Supplemental Material [33]. The

results were plotted as a function of n in Fig. 2(b). When the $\Delta P = 3$ GPa and the n increases from 1000 to 3000 and to 5000 cycles, the fraction of LRO (the transformation ratio is obtained by the ratio of the decreased a-Se area to the initial a-Se area) in a-Se increases from less than 0.5% to 11% and 24%, respectively. Moreover, the relative scattering intensity in the Raman mapping spectrum shows a similar tendency with the increase in loading cycles. Both results can prove the fraction of LRO of a-Se dependent on specific loading cycles. Note that the partial and gradual disorder-to-order transition of a-Se was also observed in the static compression experiment, while the conversion rate increased with pressure.

By way of contrast, the disorder-to-order transition sequence of a-Se under cyclic compression matches well with that under s-DAC, while its LRO component is strongly dependent on the number of loading cycles. Furthermore, the threshold pressure for the transition is significantly lower than that of static compression. This indicates that the structure order and/or molecular spatial configuration can be modified via cyclic compression-decompression. The early disorder-to-order transition is a dynamically controllable behavior, and this transformation mechanism strongly differs from previous static compression reports [10,22,23,27]. This strongly indicates that the structural order of the flexible network can be controlled and regulated by dynamic compression-decompression.

The disorder-to-order transition induced by cyclic compression-decompression is attributed to the relaxation of the amorphous structure, which can also be achieved by heating-cooling cycles [34]. However, the structural changes induced by cyclic compression-decompression are caused by mechanical stress under isothermal conditions while that induced by heating-cooling are caused by thermal activation, including changes in thermal energy and volume at atmospheric pressure [35,36]. Understanding disorder-to-order transition induced by cyclic compression-decompression is crucial to provide the complete insight into the structure relaxation in disordered system.

Several earlier studies reported an increase in the structural order for a-Se under static compression. For example, Andonov *et al.* reported that the degree of order for a-Se was promoted by applying uniaxial compression, where a little reorganization appeared in the molecule by narrowing the fluctuations amplitude of the dihedral angle γ [37]. This means uniaxial compression at one cycle contributes to the reorganization of long chains ($Z \sim 10^4$ atoms). Namely, this increase in structure order should be promoted by cyclic compression. Subsequently, Tanaka *et al.* pointed out that the changes in the structural order of a-Se before crystallization were reproduced by the evolution of second-nearest interchain distance R_2 with pressure and the width of the halo gradually decreases with increasing pressure [23]. Moreover, Katayama *et al.* investigated the effect of pressure on the local structure of a-Se via extended x-ray absorption fine structure. Their results showed that interaction within the nearest atom between adjacent chains and that within the second nearest atom within a chain strengthened with pressure increase before crystallization [13]. This may mean that the disorder-to-order transition of a-Se with pressure follows the growth of interchain ordering and spatial reorientation. Recently, Brazhkin *et al.* reported that the a-Se exhibited an inelastic behavior at about 3.5 GPa, and the weak relaxation process began at higher pressure [25]. They attribute these changes to the structure of the intermediate-range order.

In the present work, we determined that the effective pressure range for a single compression to increase the structure order is within 1 and 5 GPa. As shown in Fig. S9(a) in the Supplemental Material [33], the full width at half maximum of the diffraction halo decreases rather than increases with compression and remains almost stable when the pressure is beyond 5 GPa to the disorder-order transition at 8 GPa. Besides, a rapid reduction in the Raman scattering intensity of the 250 cm^{-1} mode can be detected within 5 GPa, denoted in Fig. S9(b) in Supplemental Material [33]. These evolutions mean the local structure can be effectively adjusted in this pressure range but the increase in the structure order is reversible at single compression. Note that the degree of order can be enhanced when the a-Se are subjected to cumulative loading cycles in this pressure range, as show in Fig. 2(a). Thus, the product of ΔP and n may be seen as a function of work, which is proportional to both ΔP and n. If the sum work done is comparable to the energy barrier of transformation, the structure order should increase. Thus, although the ΔP is decreased from 3 to 2 GPa, the structure order can also be slightly improved by increasing the number of loading cycles, as shown in Fig. S6 in the Supplemental Material [33]. Available short-range structure data on t-Se and a-Se show that the Se-Se bond length (2.37 Å, 2.32–2.36 Å) and the Se-Se-Se bond angle (103 °, 105 °) are quite similar [38,39]. However, the medium-range structural parameters between them strongly differ, especially for the ratio of correlated and uncorrelated Se chains. This difference can be quantified from the Raman vibrational band near 250 cm^{-1}. As shown in Fig. S2(b) in the Supplemental Material [33], this broad band is deconvolved into three modes, including the correlated Se chains (Corr. chains), uncorrelated Se chains (Uncorr. chains at about 250 cm^{-1}), and crowns. For the raw material, the relative ratio of uncorrelated Se-chains ratio is about 76%, and the correlated Se-chain ratio is just 10%. However, the relative ratio of uncorrelated chains gradually decreases with the increase in loading cycles while that of correlated chains gradually increases at $\Delta P = 3$ GPa, as shown in Figs. 3(a)–3(d) and in Figs. S7(a) and S7(b) in the Supplemental Material [33]. Besides, in the XRD measurements, the relative component of the second-nearest interchain R_2 gradually decreases with the loading cycles, as shown in Figs. 3(e) and 3(f) and in Figs. S7(c)–S7(e) in the Supplemental Material [33]. These changes mean the degree of order is enhanced by increasing the relative ratio of correlated chain components and decreasing the relative component R_2.

Thus, a possible mechanism for the disorder-to-order transition of a-Se in an effective pressure range is proposed, as shown in Fig. 4. Before the cyclic compression, the uncorrelated chains and R_2 were relatively dominant in a-Se, while they should decrease with the increase in cyclic compression cycles due to the irreversibility of local structural rearrangement within the effective pressure range and form a potential MRO unit. This should strengthen the intermolecular interaction and promote the growth of the interchain structural

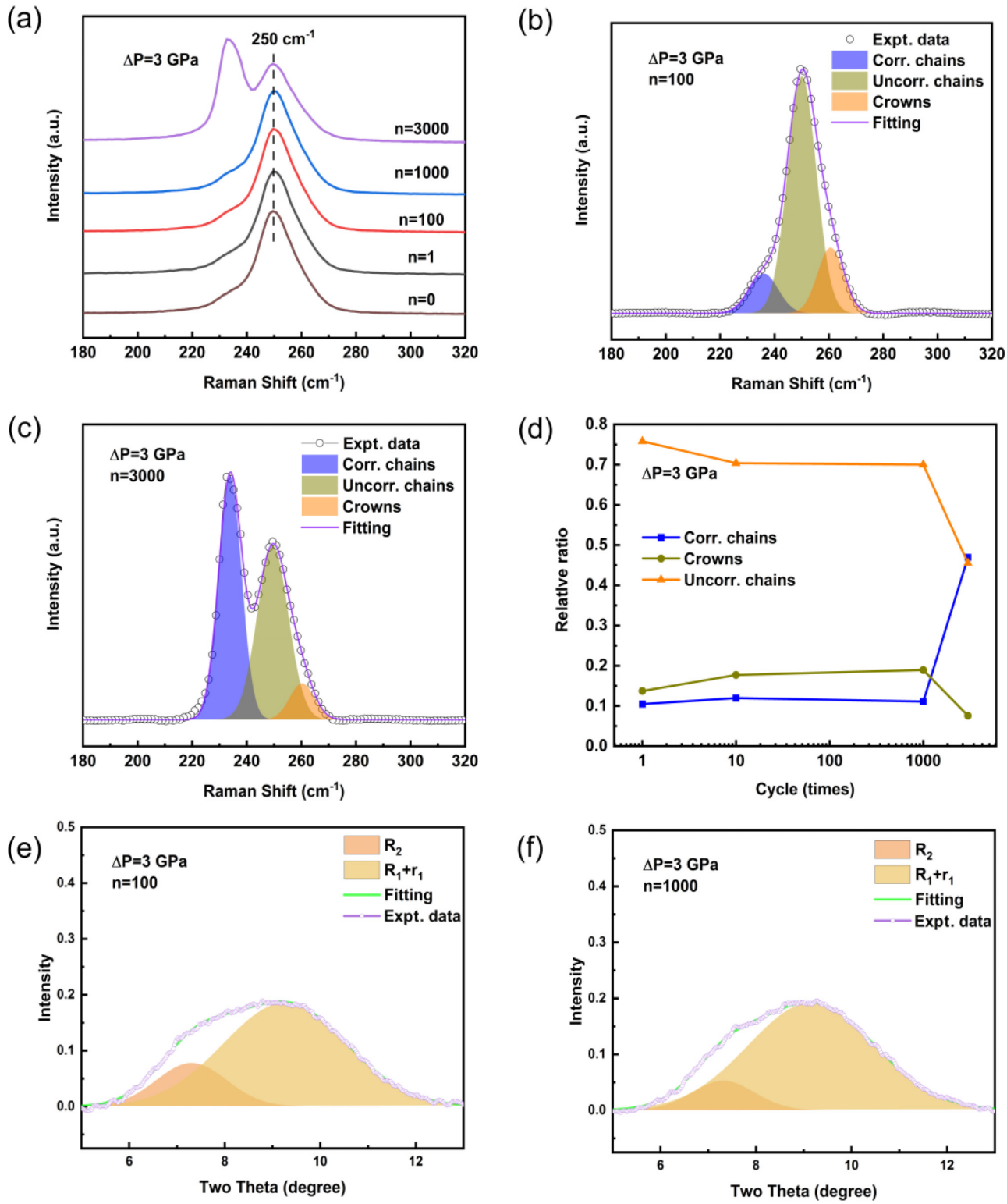

FIG. 3. Cyclic compression-decompression induced microstructure changes in the a-Se at $\Delta P = 3$ GPa (2–5 GPa). (a) The evolution of the recovered sample's Raman spectrum after different loading cycles. (b), (c) The fitting of the selected Raman spectrum. (d) The evolution of the broad-band deconvolution with different loading cycles. (e), (f) The fitting of selected XRD patterns. The halo is deconvolved into two components, including the contribution from the second-nearest interchains R_2 and that from the first-nearest interchains R_1 and intrachains r_1.

correlations, as shown in Fig. 3(d) and illustration in Fig. 4. When the relative ratio of correlated chains and intermolecular interaction of the (Se)n chains in a-Se is similar to that in t-Se, the extended MRO may form and a potential metastable state can be available [24]. Meanwhile, the reorientation and rearrangement of the Se chains in a-Se should take place. This modification in local structure should reduce the intrinsic energy barrier ΔG_s to ΔG_d during the disorder-to-order

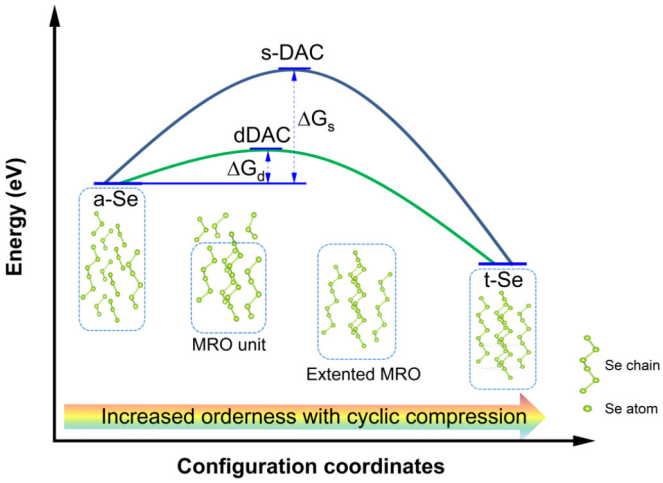

FIG. 4. Possible mechanism of the disorder-to-order transformation and the configurational energy of *a*-Se under cyclic compression at the effective pressure range. Cyclic compression should enhance interchain correlation and facilitate the chain reorientation/rearrangement, forming potential MRO units and further extended to more ordered intermediate state. Thus, the intrinsic kinetic barrier ΔG_s has been reduced to ΔG_d.

transition. Thus, when the spatial and molecular configuration of the Se chains in the *a*-Se are close to that of the (Se)*n* chains in *t*-Se during cyclic compression-decompression, the MRO structural parameters are extended to a greater length scale and the structure order increases, which causes the disorder-to-order transition.

The cyclic compression-induced disorder-order transition is an attractive result and involves highly complex processes. Besides the ratio of correlated and uncorrelated Se chains, the other MRO structure parameters, such as γ (the γ is near 100° in *t*-Se while that is distributed over a wide range 74°–112° for *a*-Se) [37], may exhibit cyclic compression-dependent modulation during the extension from the SRO to LRO and require further studies. This strategy and corresponding mechanism of tuning the degree of the order may have broader implications for the functional study of other amorphous systems, such as the toughness of metallic glass [40], topological chemical reaction [41], high-strength hydrogels [42], etc. More detailed information about this extension of the order length scale needs to be studied using *in situ* inelastic neutron and light scattering.

IV. CONCLUSION

Our work reveals that the structure order of *a*-Se can be extended to a greater length scale in an effective pressure range below the critical pressure via dDAC. This extension is achieved via the rearrangement of local structure that increases the relative component of correlated Se chains and decreases R_2 in *a*-Se, which differs from previous reports based on microcrystalline models and local density fluctuations. The degree of the disorder-to-order transformation depends on the number of loading cycles besides the increase in pressure. Thus, the amorphous solid with different degree of structure order can be accessible by this technique, which contributes to the discovery of different metastable materials and the study of formation and/or connectivity of the MRO in the disorder-order transition.

ACKNOWLEDGMENTS

This work was supported by the National Natural Science Foundation of China (Grant No. 21627802), Shanghai Science and Technology Committee, China (Grant No. 22JC1410300), and Shanghai Key Laboratory of Novel Extreme Condition Materials, China (Grant No. 22dz2260800).

[1] W. H. Zachariasen, The atomic arrangement in glass, J. Am. Chem. Soc. **54**, 3841 (1932).
[2] H. Lou, Z. Zeng, F. Zhang, S. Chen, P. Luo, X. Chen, Y. Ren, V. B. Prakapenka, C. Prescher, X. Zuo *et al.*, Two-way tuning of structural order in metallic glasses, Nat. Commun. **11**, 314 (2020).
[3] H. Tang, X. Yuan, Y. Cheng, H. Fei, F. Liu, T. Liang, Z. Zeng, T. Ishii, M.-S. Wang, T. Katsura *et al.*, Synthesis of paracrystalline diamond, Nature (London) **599**, 605 (2021).
[4] H. Tian, Y. Ma, Z. Li, M. Cheng, S. Ning, E. Han, M. Xu, P.-F. Zhang, K. Zhao, R. Li *et al.*, Disorder-tuned conductivity in amorphous monolayer carbon, Nature (London) **615**, 56 (2023).
[5] H. W. Sheng, E. Ma, H. Z. Liu, and J. Wen, Pressure tunes atomic packing in metallic glass, Appl. Phys. Lett. **88**, 171906 (2006).
[6] A. Zeidler and P. S. Salmon, Pressure-driven transformation of the ordering in amorphous network-forming materials, Phys. Rev. B **93**, 214204 (2016).
[7] Z. Fan and H. Tanaka, Microscopic mechanisms of pressure-induced amorphous-amorphous transitions and crystallisation in silicon, Nat. Commun. **15**, 368 (2024).
[8] A. Hasmy, S. Ispas, and B. Hehlen, Percolation transitions in compressed SiO_2 glasses, Nature (London) **599**, 62 (2021).
[9] M. M. J. Treacy and K. B. Borisenko, The local structure of amorphous silicon, Science **335**, 950 (2012).
[10] H. Liu, L. Wang, X. Xiao, F. De Carlo, J. Feng, H.-k. Mao, and R. J. Hemley, Anomalous high-pressure behavior of amorphous selenium from synchrotron x-ray diffraction and microtomography, Proc. Natl. Acad. Sci. USA **105**, 13229 (2008).
[11] Q. Zeng, H. Sheng, Y. Ding, L. Wang, W. Yang, J.-Z. Jiang, W. L. Mao, and H.-K. Mao, Long-range topological order in metallic glass, Science **332**, 1404 (2011).
[12] S. Lan, L. Zhu, Z. Wu, L. Gu, Q. Zhang, H. Kong, J. Liu, R. Song, S. Liu, G. Sha *et al.*, A medium-range structure motif linking amorphous and crystalline states, Nat. Mater. **20**, 1347 (2021).
[13] Y. Katayama, K. Tsuji, O. Shimomura, and H. Oyanagi, EXAFS study of amorphous selenium under pressure, J. Non-Cryst. Solids **205**, 199 (1996).
[14] L. Su, K. Shi, L. Zhang, Y. Wang, and G. Yang, Static and dynamic diamond anvil cell (s-dDAC): A bidirectional

remote controlled device for static and dynamic compression/decompression, Matter Radiat. Extremes **7**, 018401 (2022).

[15] B. Li, C. Hu, K. Shi, D. Pan, X. Zhang, L. Liu, L. Gao, S. Li, Z. Wang, G. Li *et al.*, Pressure-driven structural transformation and lattice deformation in TiB reinforced titanium matrix composites: An in-situ synchrotron x-ray diffraction study, Mater. Charact. **206**, 113411 (2023).

[16] B. Li, S. Li, K. Shi, X. Zhang, S. Yang, D. Pan, L. Liu, Y. Nan, X. Zhu, X. Song *et al.*, length Structural properties of single-walled carbon nanotubes under extreme dynamic pressures, Acta Mater. **228**, 117776 (2022).

[17] N. Duff and D. J. Lacks, Shear-induced crystallization in jammed systems, Phys. Rev. E **75**, 031501 (2007).

[18] A. V. Mokshin and J.-L. Barrat, Shear-induced crystallization of an amorphous system, Phys. Rev. E **77**, 021505 (2008).

[19] P. Yunker, Z. Zhang, K. B. Aptowicz, and A. G. Yodh, Irreversible rearrangements, correlated domains, and local structure in aging glasses, Phys. Rev. Lett. **103**, 115701 (2009).

[20] N. Nakamura, K. Inayama, T. Okuno, H. Ogi, and M. Hirao, Accelerated crystallization of colloidal glass by mechanical oscillation, Sci. Rep. **7**, 1369 (2017).

[21] J. Dong, H. Peng, H. Wang, Y. Tong, Y. Wang, W. Dmowski, T. Egami, B. Sun, W. Wang, and H. Bai, Non-affine atomic rearrangement of glasses through stress-induced structural anisotropy, Nat. Phys. **19**, 1896 (2023).

[22] S. Yuan, L. Wang, F. Liu, J. D. Bass, Y. Li, P. A. Ginsberg, D. Zhang, V. B. Prakapenka, S. Tkachev, and H. Liu, Early crystallization of amorphous selenium under high pressure studied by synchrotron XRD method, J. Phys.: Condens. Matter **35**, 264003 (2023).

[23] K. Tanaka, Structural studies of amorphous se under pressure, Phys. Rev. B **42**, 11245 (1990).

[24] Z. He, Z. G. Wang, H. Y. Zhu, X. R. Liu, J. P. Peng, and S. M. Hong, High-pressure behavior of amorphous selenium from ultrasonic measurements and Raman spectroscopy, Appl. Phys. Lett. **105**, 011901 (2014).

[25] V. V. Brazhkin and O. B. Tsiok, Glassy selenium at high pressure: Le Chatelier's principle still works, Phys. Rev. B **96**, 134111 (2017).

[26] A. Zhang, Y. Jin, T. Liu, R. B. Stephens, and Z. Fakhraai, Polyamorphism of vapor-deposited amorphous selenium in response to light, Proc. Natl. Acad. Sci. USA **117**, 24076 (2020).

[27] Z. He, X. Liu, D. Zhang, L. Zhang, and S. Hong, Pressure effect on thermal-induced crystallization of amorphous selenium up to 5.5 GPa, Solid State Commun. **197**, 30 (2014).

[28] S. Dash, P. Chen, and P. Boolchand, Molecular origin of aging of pure Se glass: Growth of inter-chain structural correlations, network compaction, and partial ordering, J. Chem. Phys. **146**, 224506 (2017).

[29] C. Prescher and V. B. Prakapenka, DIOPTAS: A program for reduction of two-dimensional X-ray diffraction data and data exploration, High Press. Res. **35**, 223 (2015).

[30] H. K. Mao, J. Xu, and P. M. Bell, Calibration of the ruby pressure gauge to 800-Kbar under quasi-hydrostatic conditions, J. Geophys. Res.: Solid Earth **91**, 4673 (1986).

[31] W. J. Evans, C.-S. Yoo, G. W. Lee, H. Cynn, M. J. Lipp, and K. Visbeck, Dynamic diamond anvil cell (dDAC): A novel device for studying the dynamic-pressure properties of materials, Rev. Sci. Instrum. **78**, 073904 (2007).

[32] S. V. Sinogeikin, J. S. Smith, E. Rod, C. Lin, C. Kenney-Benson, and G. Shen, Online remote control systems for static and dynamic compression and decompression using diamond anvil cells, Rev. Sci. Instrum. **86**, 072209 (2015).

[33] See Supplemental Material at http://link.aps.org/supplemental/10.1103/PhysRevB.111.064105 for real-time pressure measurement and the homemade compression-decompression attachments, structure characterization of a-Se, disorder-to-order transition of a-Se under static-DAC, raw 2D data at $\Delta P = 3$ GPa (2–5 GPa), structural characterization of the recovered sample after cyclic compression, XRD characterization of the recovered sample at $n = 10\,000$ for $\Delta P = 1$ or 2 GPa (4–5 GPa, or 3–5 GPa), the detailed fitting results for transforamtion ratio, microstructure changes in the a-Se caused by a single compression, as well as by cyclic compression at $\Delta P = 3$ GPa (2–5 GPa).

[34] Z. Wang, L. Liu, L. Li, X. Li, and F. Zu, Structural relaxation of $Zr_{60}Al_{15}Ni_{25}$ amorphous ribbon: Experimental evidence of the electrical resistivity, Phase Transit. **86**, 396 (2013).

[35] C. Lin, X. Liu, D. Yang, X. Li, J. S. Smith, B. Wang, H. Dong, S. Li, W. Yang, and J. S. Tse, Temperature- and rate-dependent pathways in formation of metastable silicon phases under rapid decompression, Phys. Rev. Lett. **125**, 155702 (2020).

[36] X. Zhang, H. Lou, B. Ruta, Y. Chushkin, F. Zontone, S. Li, D. Xu, T. Liang, Z. Zeng, H.-k. Mao *et al.*, Pressure-induced nonmonotonic cross-over of steady relaxation dynamics in a metallic glass, Proc. Natl. Acad. Sci. USA **120** (2023).

[37] K. Nakamura and A. Ikawa, Medium-range order in amorphous selenium: Molecular dynamics simulations, Phys. Rev. B **67**, 104203 (2003).

[38] E. H. Henninger, R. C. Buschert, and L. Heaton, Atomic radial distribution in amorphous selenium by x-ray and neutron diffraction, J. Chem. Phys. **46**, 586 (1967).

[39] R. M. Martin, G. Lucovsky, and K. Helliwell, Intermolecular bonding and lattic-dynamics of Se and Te, Phys. Rev. B **13**, 1383 (1976).

[40] H. Tang, Y. Cheng, X. Yuan, K. Zhang, A. Kurnosov, Z. Chen, W. Xiao, H. S. Jeppesen, M. Etter, T. Liang *et al.*, Toughening oxide glasses through paracrystallization, Nat. Mater. **22**, 1189 (2023).

[41] P. Zhang, D. Gao, X. Tang, X. Yang, H. Zheng, Y. Wang, X. Wang, J. Xu, Z. Wang, J. Liu *et al.*, Ordered van der waals hetero-nanoribbon from pressure-induced topochemical polymerization of azobenzene, J. Am. Chem. Soc. **145**, 6845 (2023).

[42] P. Qiao, B. Li, Y. He, K. Shi, X. Zhang, J. Zhang, Y. Wang, L. Su, Y. Chen, K. Nishinari *et al.*, High-performance hydrogels via alternate compression-decompression, J. Phys. Chem. C **126**, 21825 (2022).